Mechanical Systems and Signal Processing 84 (2017) 717–730

Contents lists available at ScienceDirect

Mechanical Systems and Signal Processing

journal homepage: www.elsevier.com/locate/ymssp

Comparison of alternatives to amplitude thresholding for onset detection of acoustic emission signals

F. Bai, D. Gagar *, P. Foote, Y. Zhao

School of Aerospace, Transport and Manufacturing, Cranfield University, Bedfordshire MK43 0AL, UK

ARTICLE INFO

Article history:
Received 4 December 2015
Received in revised form
1 September 2016
Accepted 3 September 2016

Keywords:
Onset detection
Acoustic emission
Structural health monitoring

ABSTRACT

Acoustic Emission (AE) monitoring can be used to detect the presence of damage as well as determine its location in Structural Health Monitoring (SHM) applications. Information on the time difference of the signal generated by the damage event arriving at different sensors in an array is essential in performing localisation. Currently, this is determined using a fixed threshold which is particularly prone to errors when not set to optimal values. This paper presents three new methods for determining the onset of AE signals without the need for a predetermined threshold. The performance of the techniques is evaluated using AE signals generated during fatigue crack growth and compared to the established Akaike Information Criterion (AIC) and fixed threshold methods. It was found that the 1D location accuracy of the new methods was within the range of <1–7.1% of the monitored region compared to 2.7% for the AIC method and a range of 1.8–9.4% for the conventional Fixed Threshold method at different threshold levels.

1. Introduction

Acoustic Emission (AE) detection is a Structural Health Monitoring (SHM) technique which can be used to perform continuous monitoring of structures to detect the presence of damage via permanently installed sensors. As a structure is subjected to mechanical load, AE stress waves are dynamically excited from defects such as cracks in metals or broken fibres and cracked matrix in composite materials. These waves propagate through the structure and can be detected by monitoring surface displacements at a particular location using piezoelectric or fibre optic transducers for example. In thin plate like structures these waves are also referred to as Lamb waves [1]. They typically exhibit a characteristic behaviour where their wave velocity changes with frequency. This is also known as dispersion [1]. The detection and location of damage by sensing AE signals could serve as a form of automated structural inspection, with the potential to reduce inspection time, maintenance cost and also increase availability. The location of the source of AE events (and hence the location of damage) can be determined using measurements of Time Difference of Arrival (TDOA) of the signals detected at different sensors in an array. Other inputs in the calculation are the propagating wave velocity (V_g) and the sensor coordinates (x_i, y_i) as expressed in Eq. (1) [2].

$$(x_i - x_o)^2 + (y_i - y_o)^2 = (V_g \cdot \Delta t)^2 \tag{1}$$

where,

* Corresponding author.
E-mail address: d.gagar@cranfield.ac.uk (D. Gagar).

http://dx.doi.org/10.1016/j.ymssp.2016.09.004

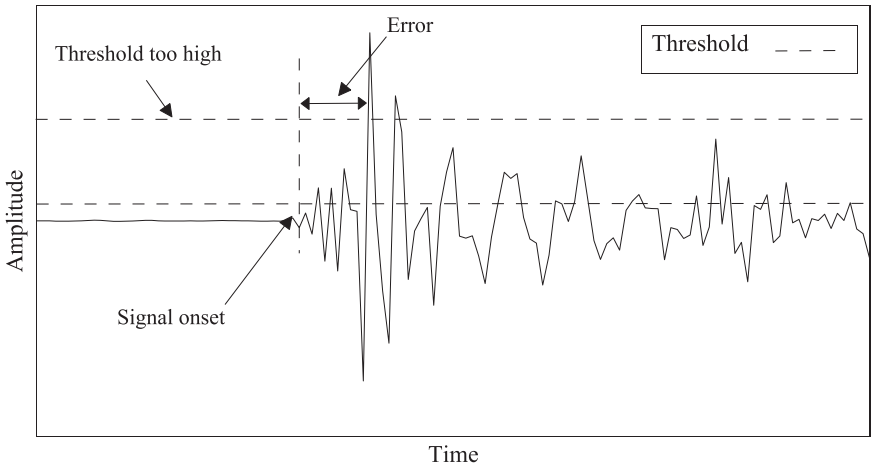

Fig. 1. Schematic of potential errors in detecting the onset of AE signals using the Fixed Threshold detection method.

x_o,y_o and (x_i, y_i) are the coordinates of source and sensors for i = 1, …n, Δt is the time difference of arrival of signal between different sensors, V_g is the propagating wave velocity.

Errors in estimating the location of damage can arise from any of these parameters. The wave velocity (V_g) for example is known to be dependent on the propagating media geometry as well as material properties; structures with complex geometry and anisotropic materials properties can be expected to experience significant variations in wave velocity even at a particular frequency. Assuming an incorrect value of wave velocity will yield errors in location estimation. Also, due to the absence of standardised approaches for sensor installation as well as human factors, inaccuracies in mapping the sensor coordinates can also yield errors in location estimation. This paper, however, is focused on the consideration of errors associated with TDOA measurements as a function of AE signal onset detection.

Currently, AE signal onset detection is most commonly performed using a fixed threshold, where the first point in time of signal amplitude exceeding a selected value marks the onset of the signal [3,4]. The main challenge in using this method is the appropriate selection of the threshold with respect to the background noise. Selecting a value too low might result in premature triggering by the preceding background noise and selecting a value too high might result in missing the time of actual signal onset as illustrated in Fig. 1. The value of detection threshold may be optimised for particular values of signal to noise ratio (SNR), if known beforehand; however in real applications a wide range of SNRs can be expected which invariably implies a vulnerability to measurement errors.

Other methods for determining the onset of AE signals have been developed in both the time as well as the time-frequency domains [2,4–9]. In the time domain, Akaike [10] developed a statistical method to determine the transition point in a time series between noise and a coherent signal, using the Akaike Information Criterion (AIC) as expressed in Eq. (2), also referred to as AIC picker [6].

$$AIC(t) = t\log_{10}(var(x[1;\ t])) + (N - t - 1)\log_{10}(var(x[t;\ N])) \tag{2}$$

This involves partitioning the signal $x(t)$ into two sections at a point t and calculating the AIC value. This process is repeated for all points within a time window of length N and the minimum value of AIC indicates the estimated point of signal onset. Sedlak, P. et al. [4] reported that the performance of this method is strongly dependent on the choice of the time window duration N. Typically, the window size N is determined by firstly using fixed threshold detection to obtain a 'rough estimation' of onset time, and then a portion of the signal - several hundred samples - is selected before and after this point as the window duration [4,6]. Improvements to the performance of this method have been demonstrated by firstly pre-processing the signal to increase the SNR and then shortening the duration of N to a smaller range. The criterion for choosing the new time window is however based on trial and error [4].

Other statistical methods have been developed in the time domain such as the Hinkley criterion [5], where the partial energy of a time series is calculated for all samples of the signal as expressed in Eqs. (3) and (4). The introduction of a negative trend δ modifies the resulting partial energy function in such a way that its global minimum is representative of the signal onset. It should be noted, however, that the parameter α is determined by trial and error; the chosen value of α can significantly influence the results obtained [6].

$$S_i' = S_i - 1\cdot\delta = \sum_{k=0}^{i} R_k^2 - i\cdot\delta \tag{3}$$

$$\delta = \frac{S_N}{\alpha \cdot N} \tag{4}$$

where S_i is the partial energy of the signal with sample number i and length N.

Kurz et al. [6] performed a study on the performance of both the Hinkley, AIC and fixed threshold methods in comparison to TDOA obtained by manual selection. The results showed that although the Hinkley method was better than the fixed threshold method, with an average of 64% of the events located within 5 mm from the manually determined location, the AIC method produced the best performance with an average of 90% of the events located within the same region.

In the time-frequency domain, one of the earlier methods was developed by Ziola and Gorman [7]. This involves cross-correlation of a recorded signal with a short Gaussian pulse at a particular frequency. The time corresponding to the peak in the correlation function is regarded as the onset of the signal at the particular frequency.

Ciampa et al. [2] applied a similar approach using Continuous Wavelet Transform (CWT) to obtain the time-frequency response, however the reference for TDOA measurements was taken from the time corresponding to the maximum of the CWT squared modulus coefficients, rather than the signal onset as typically used in other methods. A peak-searching algorithm is implemented to identify the dominant frequency for further analysis. The results show a maximum location error of less than 2%, but increasing up to 27% in the presence of reflections from the test sample edges. The source of increased error was solely attributed to the accuracy of TDOA measurements. This suggests that TDOA analysis based on a single frequency becomes less reliable in the presence of reflections from boundaries and features, which are integrally part of real structures [11]. Eaton et al. [3] also noted that the variation in frequency content and mode amplitude as a function of source orientation can introduce further errors.

Although a number of alternative methods to the commonly used fixed threshold crossing have been developed, they often tend to depend on some forms of predetermined threshold determined by trial and error [4,6] or inherently unstable [3,11]. On the other hand, the amplitude threshold-dependent method is apparently unstable in the presence of noise. The objective of this paper is to, therefore, develop novel threshold-free methods for AE signal onset detection and determine their performance in comparison to the established AIC and fixed threshold methods in the presence of noise at various levels.

2. Methodology

Three new methods have been developed to perform AE signal onset detection and TDOA measurements based on analyses in the time domain and the time-frequency domain.

2.1. Time-varying correlation method

This method is based on cross-correlation and the surrogate significance test in the time domain to automatically determine the onset of AE signals.

Cross-correlation is a measure of the linear correlation (dependence) between two signals, giving a value between $+1$ and -1 inclusive, where 1 is total positive correlation, 0 is no correlation, and -1 is total negative correlation. Consider two signals $U = u(1), u(2), \ldots u(n)$ and $V = v(1), v(2), \ldots v(n)$, the cross-correlation between these two signals can be calculated using the expression in Eq. (5).

$$r_{uv}(d) = \frac{\sum_{i=1}^{n}(u(i) - \overline{U})(v(i-d) - \overline{V})}{\sqrt{\sum_{i=1}^{n}(u(i) - \overline{U})^2}\sqrt{\sum_{i=1}^{n}(v(i) - \overline{V})^2}} \tag{5}$$

where $\overline{U}$ and $\overline{V}$ are the means of the signals U and V respectively, n is the number of samples, and $d = 0, 1, 2, \ldots n-1$ is the time delay. The magnitude of the cross-correlation function $r_{uv}(d)$ represents the level of similarity between these two signals with the time shift and the maximum value k, as expressed in Eq. (6), indicates the time when both signals are aligned with the most similar characteristics.

$$k = \underset{d}{\operatorname{argmax}}(r_{uv}(d)) \tag{6}$$

The time-varying correlation method is a variant of the traditional cross-correlation, performed using a sliding window centred at position t and with duration h; the selection of h can be expected to affect the reliability of the results obtained to a certain extent. A large value of h would produce a robust cross-correlation of the signals, however at the expense of increased computation requirements. Conversely, choosing a small value of h will reduce the computation requirement but with relatively reduced reliability. The principle is to choose a window size as small as possible with minimal computation requirement.

The level of correlation at time t is denoted by $s(t)$ and expressed in Eq. (7).

$$s(t) = \underset{d}{\operatorname{argmax}}(r_{uv}(t, d)) \tag{7}$$

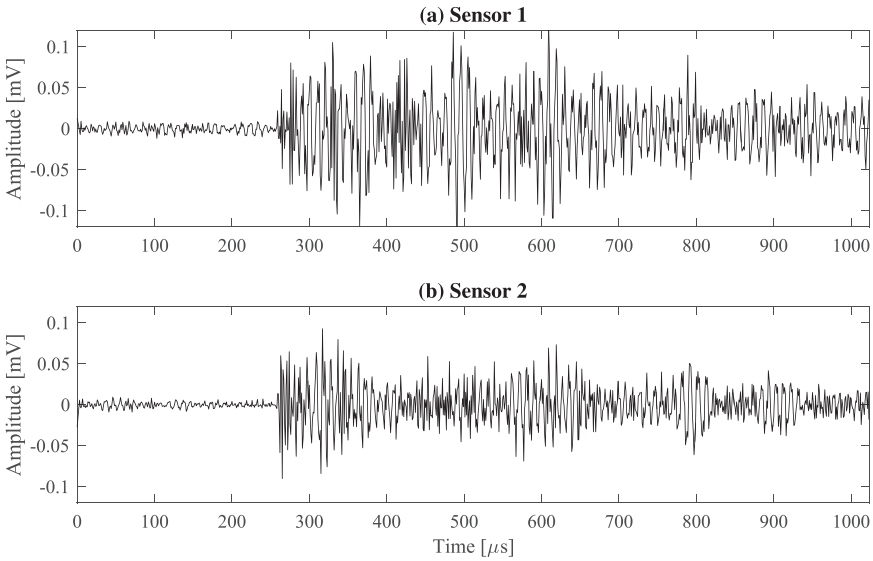

Fig. 2. AE signals from the same event recorded by a pair of sensors at different locations.

where,

$$r_{uv}(t, d) = \frac{\sum_{i=t-h/2}^{t+h/2}(u(i) - \overline{U})(v(i-d) - \overline{V})}{\sqrt{\sum_{i=t-h/2}^{t+h/2}(u(i) - \overline{U})^2}\sqrt{\sum_{i=t-h/2}^{t+h/2}(v(i) - \overline{V})^2}} \tag{8}$$

The maximum of the function $s(t)$ is similarly indicative of the time when both signals are aligned with the most similar characteristics. Fig. 3 shows the cross-correlation series for AE signals recorded by a pair of sensors, as shown in Fig. 2, with different distances from the AE event source location.

The onset time of a signal corresponds to the point where there is a significant step change in the series of the time-varying correlation function $s(t)$. This can be automatically detected using the Surrogate significance test [12–14]. This is a statistical technique used to detect non-linearity in a time series. Assuming the signal U is related to the signal V, this sort of dependence is lost when V is re-ordered randomly. The order of the data in V is randomised by a shuffle procedure that saves the distribution properties of the signal V, but destroys the temporal relationship between U and V. In this paper, an Amplitude Adjusted Fourier Transform (AAFT) randomization surrogate technique [13] is applied. This is done by performing a Fourier transform of the signal V using its randomised phase whilst preserving the amplitude in the process. The surrogate version of the original signal is generated by applying the inverse Fourier transform and referred to as the surrogate signal. The time-varying correlation between the signal U and the surrogate data is then calculated. This procedure is repeated 100 times to achieve statistical significance as suggested in reference [15]. The correlation series for the surrogate signal, denoted by $\tau(t)$, is defined as the 95% quantile of 100 tests for each time step t. Searching from the time when $s(t)$ reaches the maximum toward the left direction, the TOA for the signal U is represented by the first time when $s(t)$ is below $\tau(t)$. As shown in Fig. 3(a), the blue plot illustrates $s(t)$ and red curve plots $\tau(t)$, and the TOA is determined as 247 μs.

By swapping the signal U for V, the TOA for the signal V can be detected, as illustrated by Fig. 3(b). The value of TDOA is finally calculated using Eq. (9).

$$TDOA(U, V) = |TOA_U - TOA_V| \tag{9}$$

Different window sizes h ranging from 32 to 124 sample points were tested in performing the cross-correlation of the signals illustrated in Fig. 3 and the coefficient of variation was calculated as 5.8%. This is considered insignificant. In this paper, a window size h of 32 sample points was selected.

2.2. CWT-based correlation method

This method is based on cross-correlation and the surrogate significance test in the time-frequency domain to automatically determine the onset of AE signals. Continuous wavelet transform (CWT) is used to produce a spectrum of time-frequency according to the relationship between the scale and the frequency. Unlike the conventional Fourier transform, CWT possess the ability to construct a time-frequency representation of a signal that offers good time and frequency localisation, which helps detect the accurate location of the time when the frequency distribution significantly changes. Considering a signal $u(t)$, the coefficient of its CWT at a scale $a(a > 0, a \in \mathbb{R})$ and translational value $b \in \mathbb{R}$ is expressed as:

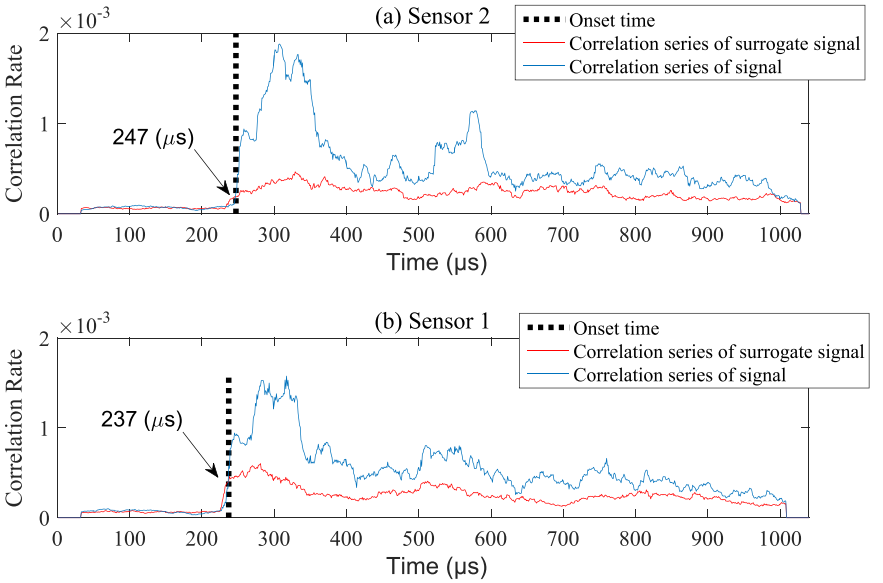

Fig. 3. AE signal onset detection using the Time-varying correlation method for (a) sensor 1 and (b) sensor 2. The blue line indicates the correlation series of the raw signals and red line is for correlation series of surrogate signals. (For interpretation of the references to color in this figure legend, the reader is referred to the web version of this article.)

$$c(a, b; x(t), \phi(t)) = \int_{-\infty}^{\infty} x(t)\frac{1}{\sqrt{a}}\phi^*\left(\frac{t-b}{a}\right)dt \tag{10}$$

where $\phi(t)$ is a continuous function in both time and frequency domains called the mother wavelet and the * represents the operation of complex conjugate. CWT coefficients are not only under the influence of scale and translational values, but also the type of mother wavelet. The selection of an appropriate mother wavelet often depends on the feature of the signal to be analysed. In this study, different types of mother wavelet have been tested and compared. Due to its superior performance, the complex Morlet wavelet was used through this paper. Fig. 4 shows the CWT spectrum of the pair of AE signals shown in Fig. 2.

The CWT-based correlation method basically involves performing cross-correlation of the CWT coefficients for consecutive time samples of a signal. The frequency distribution of an AE signal at any time before signal onset is known to be pseudo-random and, therefore, the correlation between CWT coefficients for two consecutive time samples in this period can be expected to be low. In contrast, the frequency distribution of an AE signal at any time after the signal onset is relatively coherent due to its inherent periodicity, which also suggests that the correlation between CWT coefficients for two consecutive time samples in this period is high. The blue plots in Fig. 5 show the cross-correlation series of the CWT coefficients for the AE signals shown in Fig. 2.

The onset of a signal corresponds to the point where there is a significant step change in the cross-correlation of the CWT coefficients. The Surrogate significance test is also applied, as previously described in Section 2.1, to automatically determine the onset time of the signals. Fig. 5 shows the cross-correlation series of the CWT coefficients for the surrogate signals, illustrated by the red plots.

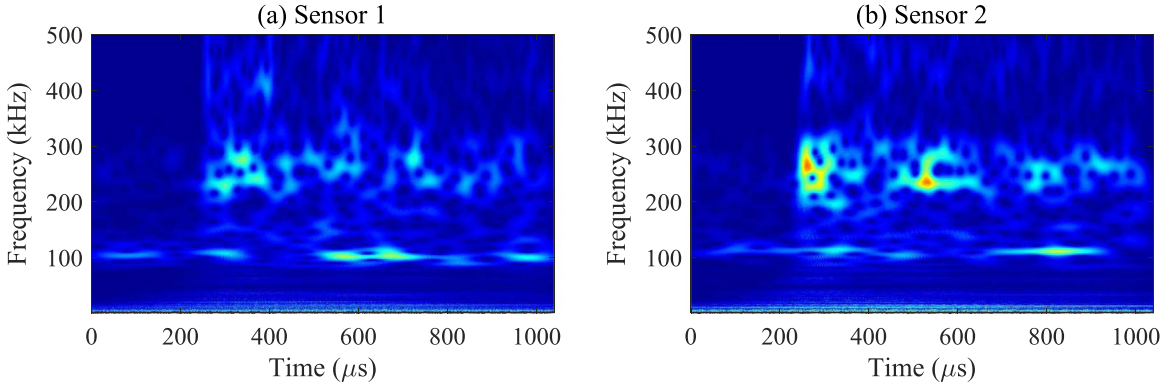

Fig. 4. CWT spectrum for AE signals recorded by a pair of sensor with different distances from the AE event location.

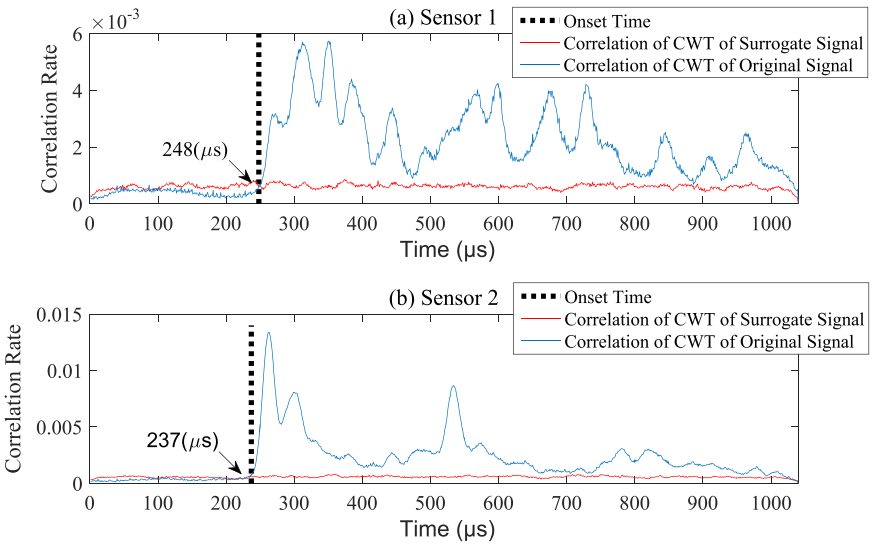

Fig. 5. AE signal onset detection using the CWT-based correlation method for (a) sensor 1 and (b) sensor 2. The blue line indicates the correlation series of the raw signal and red line is for correlation series of surrogate signal. (For interpretation of the references to color in this figure legend, the reader is referred to the web version of this article.)

The CWT-based correlation method can be summarised as the following steps.

1. Calculate the time-frequency response for the signal U based on CWT.
2. Calculate the time-varying correlation between two consecutive columns of CWT coefficients, denoted as $w_U(t)$.
3. Generate the surrogate signal and apply step 1–2.
4. Repeat step 3 for 100 times and the 95% quantile of all tests at each time is chosen as the surrogate threshold, denoted as $\tau_U(t)$.
5. Searching from the time when $w_U(t)$ reaches the maximum toward the left direction, the TOA for the signal is indicated by the first time when $w_U(t)$ is below $\tau_U(t)$.
6. Repeat step 1–5 for the next signal V.
7. Calculate the TDOA based on the function (9).

2.3. CWT-based binary map

This method utilises the CWT coefficients of an AE signal's time-frequency response to construct a greyscale image, with the magnitude of each component representing the intensity of a pixel. The presence of noise in the image is minimised by applying a Median filter [16]. This is a nonlinear digital filtering technique where the intensity of each pixel is replaced by the median intensity of the neighbouring pixels.

The onset of the signal is determined by performing an image segmentation to create clear contrast in its features, from which the leading edge can be identified. This involves converting the greyscale image to a binary image where each pixel is assigned a value of 0 or 1 depending on whether its intensity exceeds or falls below an optimal level. The Otsu's method is used to automatically determine the optimal intensity level at which the intra-class variance is minimum and the inter-class variance is maximum [17]. The weighted within-class variance is expressed in Eq. (11).

$$\sigma_w^2(g) = q_1(g)\sigma_1^2(g) + q_2(g)\sigma_2^2(g) \tag{11}$$

Where the class probabilities are estimated as:

$$q_1(g) = \sum_{i=1}^{g} P(i), \quad q_2(g) = \sum_{i=g+1}^{g} P(i) \tag{12}$$

The class variances and mean are given as:

$$\sigma_1^2(g) = \sum_{i=1}^{g} [i - \nu_1(g)]^2 \frac{P_i}{q_1(g)}, \quad \sigma_2^2(g) = \sum_{i=g+1}^{g} [i - \nu_2(g)]^2 \frac{P_i}{q_2(g)} \tag{13}$$

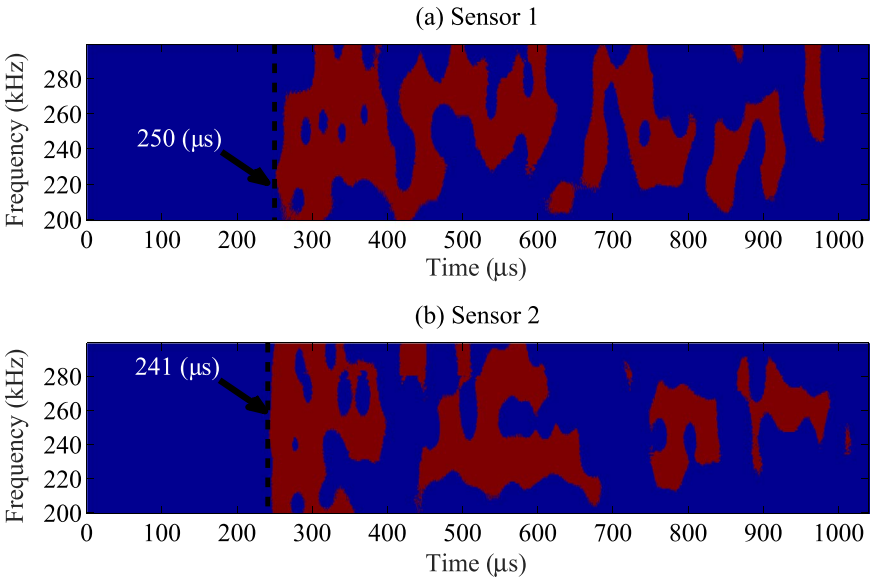

Fig. 6. AE signal onset detection using the CWT-based binary map method for (a) sensor 1 and (b) sensor 2.

$$\nu_1(g) = \sum_{i=1}^{g} \frac{iP(i)}{q_1(g)}, \quad \nu_2(g) = \sum_{i=g+1}^{g} \frac{iP(i)}{q_2(g)} \tag{14}$$

where $_{Pi}$ denotes the probability of the grey level i.

The algorithm iteratively computes the value $\sigma_w^2(g)$ for all possible intensity level g (normally from 0 to 255). The g that has the maximum σ_w^2 is selected as the threshold to create the binary map image.

The onset time of an AE signal can therefore be determined by finding the leftmost non-zero pixel in the binary image. The effectiveness of the method may be improved by applying in a band of frequency which can be specified if the frequency characteristics of the AE signal are known. Fig. 6 shows an example of a binary map image generated for a pair of AE signals with indications of their respective onset times.

The CWT based binary map method can be summarised as:

1. Calculate the time-frequency response for the signal U based on CWT.
2. Normalise the power spectrum to generate a grey-scale image.
3. Reduce noise using a Median filter.
4. Generate a binary map using the Otsu's method.
5. Detect the earliest non-zero pixel to represent the TOA for the signal.
6. Repeat step 1–5 for the next signal V.
7. Calculate the TDOA.

3. Experiments

An experiment in which AE signals were generated by growing cracks in a metal specimen undergoing mechanical fatigue was performed in order to evaluate and compare the three TDOA measurement methods described above. A fatigue crack growth test was performed on a Single Edge Notch (SEN) 2014 T6 aluminium sample with thickness of 2 mm as illustrated in Fig. 7. The sample was subjected to constant amplitude fatigue loading with stress range of 52 MPa, stress range of 0.1 and frequency of 2 Hz.

A multi-channel Physical Acoustics AE system (PCI-2) was used to record AE signals using broadband piezoelectric sensors (WDI), at positions as indicated in Fig. 7, with sampling rate of 1 MS/s and a pre-amplifiers with band-pass frequency filters in the range of 20–1200 kHz. The fixed detection threshold was set at 45 dB and the pre-amplifier gain for each channel was set to 40 dB; the magnitude of the signals was determined with reference to 1 μV as expressed in Eq. (15).

$$dB_{AE} = 20\log_{10}\left[\frac{A}{1\mu V}\right] - dB_{PG} \tag{15}$$

where,

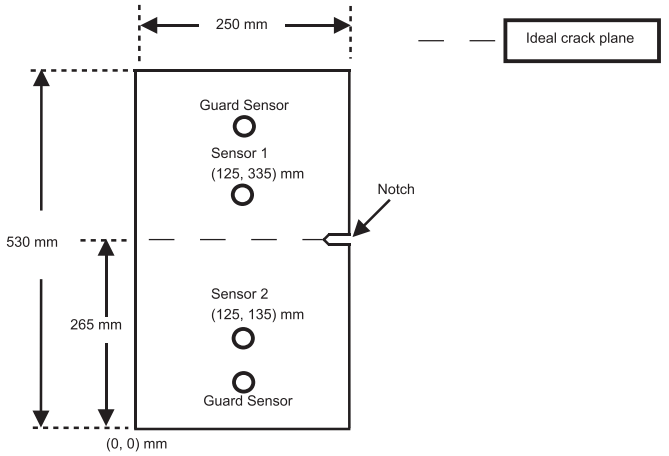

Fig. 7. Test sample geometry and layout of AE sensors.

A – Voltage measurement
dB_{PG} – Preamplifier gain

Exclusive monitoring of AE signals generated from the fatigue crack was achieved by implementing a spatial filter set to reject spurious signals generated from the test machine grips using guard sensors, illustrated in Fig. 7; acquisition using Sensors 1 and 2 is disabled for 1 ms once an extraneous AE signal is detected by the guard sensors.

4. Results

AE signals were recorded throughout the test, from fatigue crack initiation until final failure, and a total of 111 AE events were randomly selected for further analysis. Measurements of the TDOA for all the AE events were determined using each of the three threshold-independent methods previously described, alongside the already established AIC [6] and the fixed threshold methods. Analysis using the AIC method was performed with a window size N of 800 μs, as defined in Eq. (2).

4.1. Accuracy and precision

The 1-Dimensional location error with reference to the crack plane was calculated for each of the five methods using the expression in Eq. (16).

$$d_{location} = \frac{D - (\Delta t^{*} V)}{2} - d \tag{16}$$

where,

D – Distance between sensors
Δt – Time difference of arrival
V – Wave velocity
d – Distance to closest sensor

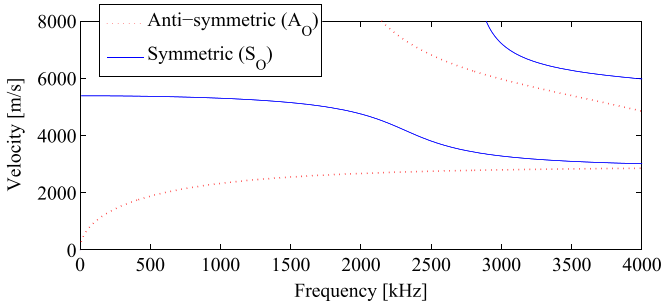

Fig. 8. Dispersion relation for the fundamental Lamb wave modes in 2 mm thick 2014-T6 Aluminium.

Table 1
Number of AE events located within the range of expected location estimates using various methods.

	Binary Map	CWT-based correlation	Time-varying correlation	AIC	Fixed threshold		
					40 dB	45 dB	50 dB
Number of AE events	105	99	106	108	102	83	48

Theoretical values for the propagating wave velocity were assumed. The dispersion relation for the fundamental wave modes is shown in Fig. 8, obtained using Wavescope [18]. The average wave group velocity for frequencies up to 400 kHz is 5321 m/s $\pm$ 81.5.

Given the layout of the sensors with respect to the crack plane, shown in Fig. 7, the maximum possible location error is limited by the respective distance between the crack plane and each sensor, given an average wave velocity of 5321 m/s; this corresponds to a maximum of 70 mm towards Sensor 1 and 130 mm towards Sensor 2. The numbers of AE events with location estimates within the range of maximum expected errors are shown in Table 1 for the threshold-independent methods and the Fixed Threshold method at various levels of threshold. It can be seen that as the threshold level increased the number of AE events located within the range of expected errors consistently decreases. At a threshold level of 50 dB the number of AE events registered was less than half of those for all the threshold-independent methods. The greatest number of AE events was observed in the case of the AIC method.

The results for the distribution of the range of location estimates are shown in Fig. 9 for the various threshold-independent methods and Fig. 10 for the Fixed Threshold method at different threshold levels; the origin (at 0 mm) represents the true location of the fatigue crack plane. It can be seen that although the distributions are typically multi-modal, the most dominant mode is centred in the vicinity of the crack location for the case of the location estimates obtained using the

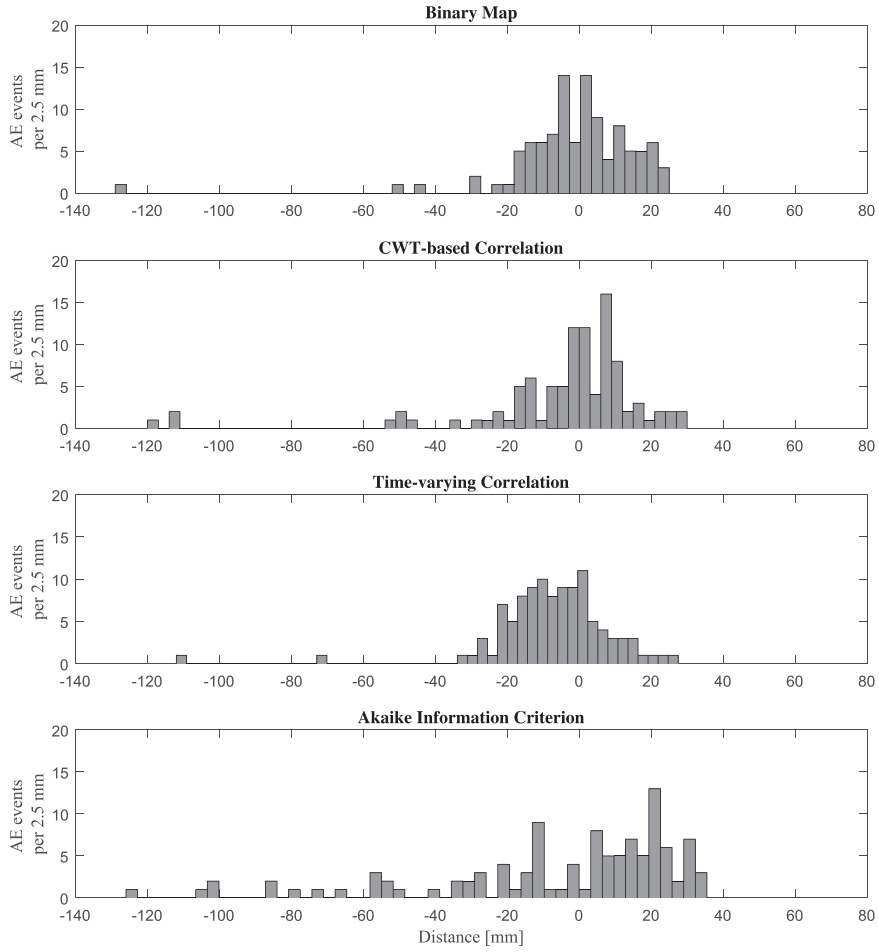

Fig. 9. Distribution of 1-Dimensional location estimates using various threshold-independent methods.

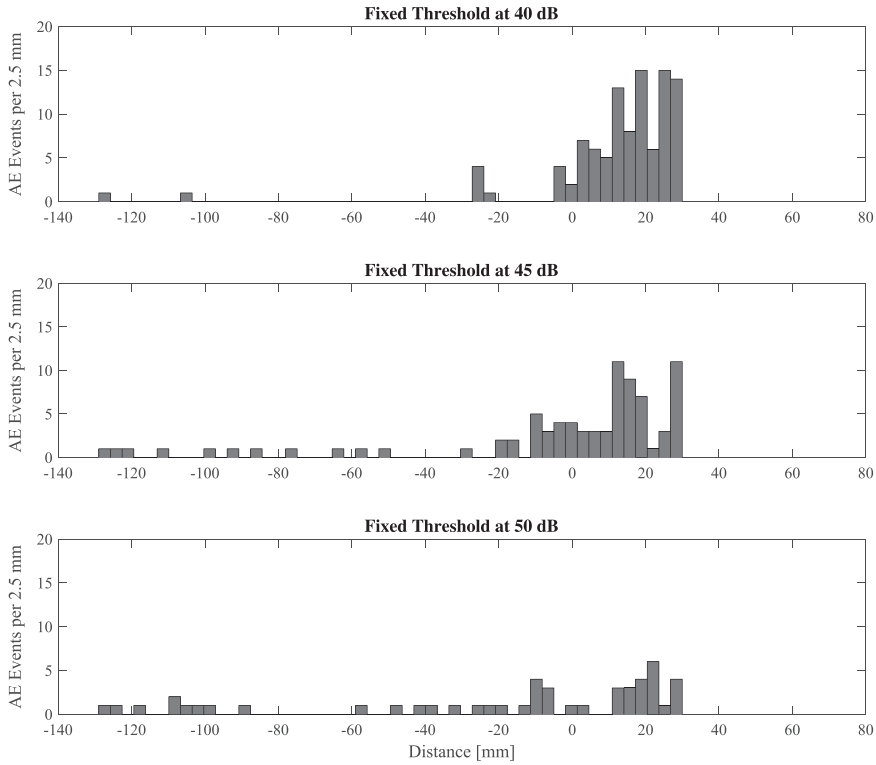

Fig. 10. Distribution of 1-Dimensional location estimates using the Fixed Threshold method at different threshold levels.

Binary Map and the CWT-based correlation methods. In contrast, the dominant mode for the Fixed Threshold method at all the threshold levels is about 20 mm away from the actual crack location.

The Mean Absolute Error (MAE), as expressed in (17), and corresponding standard deviations (σ) were calculated for each of the distributions as a measure of location accuracy and precision. For the threshold-independent methods, it was observed that in terms of location accuracy the Binary Map method produced the least mean absolute location error of 1.1 mm and the Time-varying correlation method produced the largest mean absolute location error of 7.4 mm as shown in Table 2. In the case of the Fixed Threshold method, it can also be seen that the MAE both increases and decreases with increasing threshold level.

$$MAE = |\frac{\sum_{i=1}^{N} x(i)}{N}| \tag{17}$$

where,

x – Location error

In terms of location precision, the CWT-based Correlation method produced the least spread in the distribution with a standard deviation of 16.6 mm. The Fixed Threshold method showed a trend of increasing standard deviation with increased threshold level.

Table 2
Comparison of accuracy and precision of the distribution of errors in AE event location estimates obtained with the various methods.

		Accuracy MAE [mm]	Precision Standard deviation [mm]
Binary Map		1.1	18.2
CWT-based correlation		4.7	16.6
Time-varying correlation		7.4	25.0
AIC		5.3	34.8
Fixed threshold	40 dB	11.9	22.2
	45 dB	3.5	38.3
	50 dB	18.8	49.1

Table 3
Comparison of average processing time per AE event using the various methods.

Method	Processing time [s]
Binary Map	0.22
CWT-based correlation	69.53
Time-varying correlation	38.57
AIC	0.12

The average processing time per AE event using the various techniques is shown in Table 3. This was obtained using a standard PC by averaging 111 tests. It can be seen that the AIC method is relatively the least computationally intensive, whereas the CWT correlation method required the most time for computation. However, the computational time can be significantly reduced for both the CWT-based correlation method and the Time-varying correlation method by reducing the repetition times for surrogate tests. A number of tests have been conducted and the result shows that he repetition times of 30 is sufficient to produce reliable results.

4.2. Robustness to noise

In this section, the performance of the various methods in terms of measurement accuracy in the presence of increasing levels of noise is investigated. To achieve this, simulated noise was artificially added (digitally) with varying amplitude levels to actual sensor signals of a fixed amplitude. For each new SNR the effectiveness of the five TDOA measurement methods could be compared. Twenty signals from the dataset with nominal SNR greater than 10 dB were randomly selected as the subject of this study. The SNR was calculated using the expression in Eq. (18).

$$SNR_{dB} = 20\log_{10}\frac{\sum_{i=1}^{n} A_{signal}(i)}{\sum_{i=1}^{n} A_{noise}(i)} \tag{18}$$

where,

A – Amplitude
n – Length of signal

The noise is considered to be the portion of the signal preceding the onset point t which was visually identified.

Reduction in SNR was achieved by adding a noise signal with increasing amplitude scaling factors to the original signal. The additive noise signal was created by duplicating and cascading stochastic copies of the noise time series from the original signal until the same length as the original signal was obtained. The surrogate technique as previously described in Section 2.1 was applied to the additive noise signal to eliminate the artificial periodicity introduced from repetitions in the original noise time series, whilst preserving its frequency vs amplitude distribution. This process was applied to the previously selected signals to generate 3 new signals at each level of SNR. An example is illustrated in Fig. 11; the time-frequency response of the signals is also shown and a similar frequency distribution in the range less than 150 kHz can be seen for the various SNR.

Table 4 shows the performance in terms of average location accuracy for the 20 independent AE events using all threshold-independent methods as well as the Fixed Threshold method, at nominal value of 45 dB, with decreasing levels of SNR. It can be seen that all the threshold-independent methods exhibited a trend of progressively deteriorating average location error with decreasing SNR. The Fixed Threshold method on the other hand showed an erratic behaviour where the average location error was observed to both increase and decrease with decreasing SNR. The largest average location errors were observed for the case of the Fixed Threshold method with a maximum of 96.5 mm at an SNR of 5 dB. This is equivalent to 48% of the monitored region. The least average location error was observed for the Binary Map method with a minimum of 0.5 mm at an SNR of 10 dB, which represents <1% of the monitored region.

The range of location estimates for each of the methods were also calculated and shown in Table 5 as a measure of stability in performance. It can be seen that the Binary Map produced the smallest range of location estimates and the CWT-based Correlation method produced the largest in contrast.

5. Discussion

The results have shown that for representative AE signals the Binary Map method yielded improved 1D location accuracy compared with the established AIC and amplitude threshold methods. The threshold-independent techniques produced Mean Absolute Errors in the range 1.1–7.4 mm, with 5.3 mm for the AIC method. In contrast, the amplitude threshold method produced errors oscillating in the range 3.5–18.8 mm at different threshold levels. From this it can be concluded that some improvement in accuracy of location of AE events could be gained using the threshold-independent methods with the binary map technique producing the lowest error for these tests.

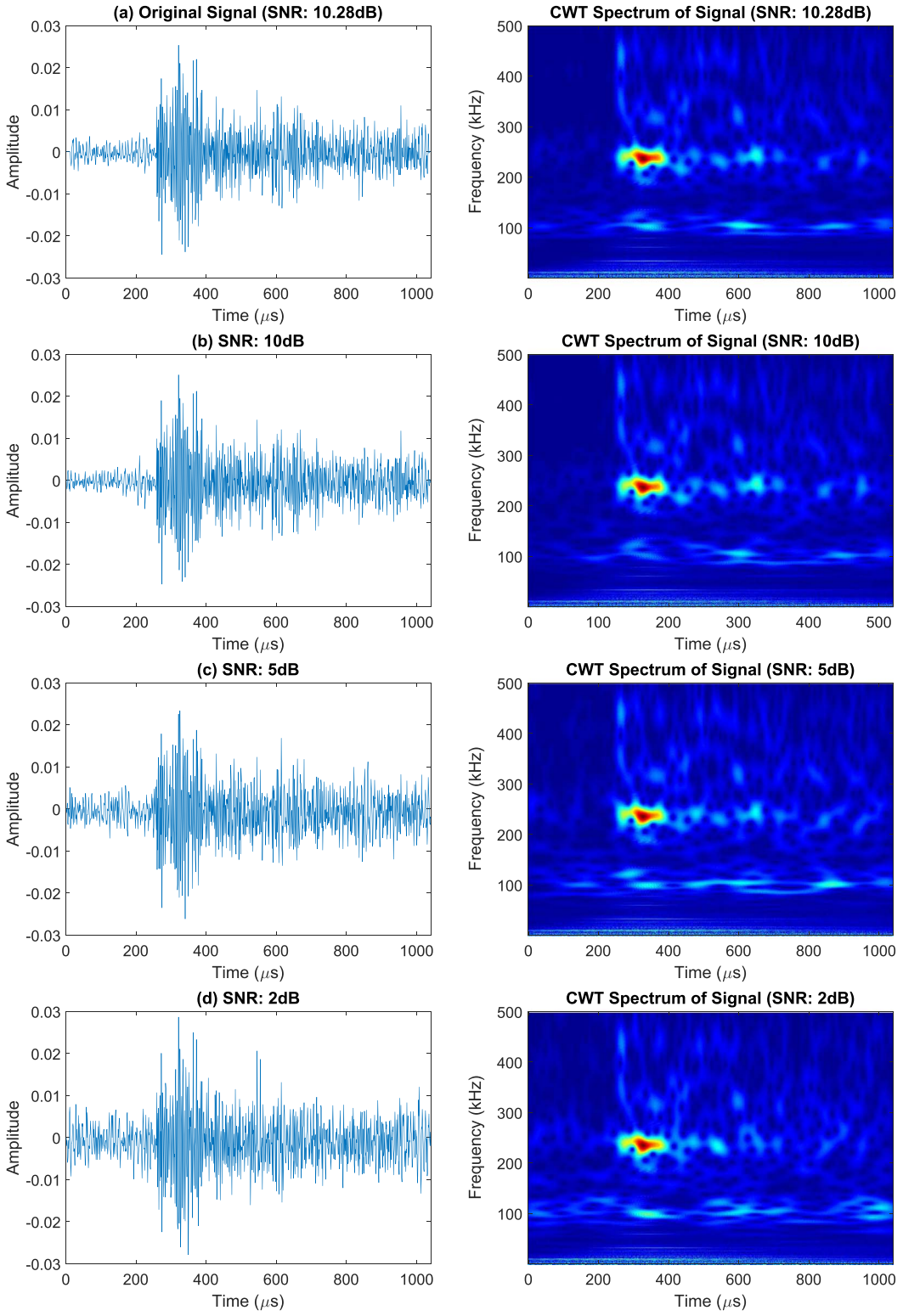

Fig. 11. (a)–(f) AE signal at different SNR values with corresponding time-frequency response.

The potential benefits of threshold-independent methods is more pronounced as the SNR quality of typical AE signals deteriorates. In this test when the SNR is reduced for a set of AE signals from 20 different events, the fixed threshold method yielded average location errors oscillating between 48.1 and 96.5 mm. For the same levels of signal deterioration, the

Table 4
Comparison of average location accuracy for 20 AE events with decreasing SNR using the different onset detection methods.

SNR	10 dB	5 dB	2 dB
	Mean absolute error [mm]		
Time-varying correlation	9.5	28.1	51.9
CWT-based correlation	3.5	31.1	67.5
Binary Map	0.5	8.6	12.3
AIC	3.7	14.8	17.5
Fixed threshold @ 45 dB	48.1	96.5	50.3

Table 5
Comparison of stability (difference between minimum and maximum MAE) with decreasing SNR for the five AE signal onset detection methods.

Method	Range [mm]
Time-varying correlation	42.4
CWT-based correlation	64
Binary Map	11.8
AIC	13.8
Fixed threshold @ 45 dB	46.2

threshold-independent techniques yielded relatively smaller increases in location error, with an exception of the CWT-based correlation method at SNR of 2 dB. The smallest variation was from the Binary Map method which showed increase in location error from 0.5 to 12.3 mm.

From these experimental tests, it is clear that the threshold free methods for determination of AE source location demonstrate greater robustness to noise (signal deterioration) than the standard amplitude threshold methods that currently prevail in applications using AE.

The significance for applications using AE detection as a form of structural heath monitoring is that sensors once installed, demonstrate ageing or degradation during their lifetimes, such that sensor SNR are degraded, may still provide useable measurement accuracy depending on the system performance requirements. Use of threshold free techniques such as developed and demonstrated in this paper could therefore constitute a mitigation strategy for sensor degradation over their operating lifetimes.

6. Conclusions

1. Three new AE signal onset detection techniques have been developed in the time and time-frequency domains with 1D location accuracy ranging from <1% to 7.1% of the monitored region compared to 2.7% for the AIC method and a range of 1.8–9.4% for the conventional Fixed Threshold method at different threshold levels.
2. The new methods presented perform onset detection without the need for predetermined or assumed thresholds.
3. The Binary Map method for AE event location developed and described in this paper demonstrates substantial robustness to degraded signal quality when compared with current fixed amplitude threshold methods.

Acknowledgement

This work was supported by the EPSRC Centre for Innovative Manufacturing in Through-life Engineering Services (Grant number EP/I033246/1).

Enquiries for access to the data referred to in this article should be directed to researchdata@cranfield.ac.uk.

References

[1] J.L. Rose, Waves in Plates, in: Ultrasonic Waves in Solid Media, Cambridge, 1991, p. 101.
[2] F. Ciampa, M. Meo, Acoustic emission source localisation and velocity determination of the fundamnetal mode A0 using wavelet analysis and a Newton-based optimisation technique, Smart Mater. Struct. 19.
[3] M.J. Eaton, R. Pullin, K.M. Holford, Towards improved damage location using acoustic emission, in: Proceedings of the Institution of Mechanical Engineers, Part C: Journal of Mechanical Engineering Science, 226(9), 2012, pp. 2141–2153.
[4] P. Sedlak, Y. Hirose, M. Enoki, Acoustic emission localization in thin multi-layer plates using first-arrival determination, Mech. Syst. Signal Process. 36 (2) (2013) 636–649.

[5] D.V. Hinkley, Inference about the change-point from cumulative sum tests, Biometrika 58 (3) (1971) 509–523.
[6] J.H. Kurz, C.U. Grosse, H.W. Reinhardt, Strategies for reliable automatic onset time picking of acoustic emissions and of ultrasound signals in concrete, Ultrasonics 43 (7) (2005) 538–546.
[7] S.M. Ziola, M.R. Gorman, Source location in thin plates using cross-correlation, J. Acoust. Soc. Am. 90 (5) (1991) 2551–2556.
[8] P. Earle, P. Shearer, Characterization of global seismograms using an automatic-picking algorithm, Bull. Seismol. Soc. Am. 84 (2) (1994) 366–376. cited By 123.
[9] T. Lokajek, K. Klma, A first arrival identification system of acoustic emission (ae) signals by means of a high-order statistics approach, Meas. Sci. Technol. 17 (9) (2006) 2461.
[10] H. Akaike, Markovian representation of stochastic processes and its application to the analysis of autoregressive moving average, Ann. Inst. Stat. Math. 26 (1) (1974) 363–387.
[11] M.A. Hamstad, A. O'Gallagher, J. Gary, A wavelet transform applied to acoustic emission signals: part 2: source location, J. Acoust. Emiss. 20 (2002) 62–82.
[12] D. Prichard, J. Theiler, Generating surrogate data for time series with several simultaneously measured variables, Phys. Rev. Lett. 73 (7) (1994) 951–954, http://dx.doi.org/10.1103/PhysRevLett.73.951.
[13] J. Theiler, S. Eubank, A. Longtin, B. Galdrikian, J. Doyne Farmer, Testing for nonlinearity in time series: the method of surrogate data, Physica D: Nonlinear Phenom. 58 (1–4) (1992) 77–94, http://dx.doi.org/10.1016/01672789(92)90102-S.
[14] Y. Zhao, S.A. Billings, H. Wei, Tracking time-varying causality and directionality of information flow using an error reduction ratio test with applications to electroencephalography data, Phys. Rev. E 86 (2012) 051919.
[15] T. Schreiber, A. Schmitz, Surrogate time series, Physica D: Nonlinear Phenom. 142 (34) (2000) 346–382, http://dx.doi.org/10.1016/S0167-2789(00)00043-9.
[16] T.S. Huang, G.J. Yang, G.Y. Tang, A fast two-dimensional median filtering algorithm, IEEE Trans. Acoust. Speech Signal Process. 27 (1) (1979) 13–18, http://dx.doi.org/10.1109/TASSP.1979.1163188.
[17] N. Otsu, Threshold selection method from gray-level histograms, IEEE Trans. Syst. Man Cybern. (1) (1979) 62–66. SMC-9.
[18] L.f.A.M. (LAMSS), S. Structures, WAVESCOPE: Dispersion curves, Group velocities and Tuning for metallic structures.

2016-10-10

Comparison of alternatives to amplitude thresholding for onset detection of acoustic emission signals

Bai, F.

Elsevier

F. Bai, D. Gagar, P. Foote, Y. Zhao, Comparison of alternatives to amplitude thresholding for onset detection of acoustic emission signals, Mechanical Systems and Signal Processing, Volume 84, Part A, 1 February 2017, pp.717-730

http://dx.doi.org/10.1016/j.ymssp.2016.09.004